

# H-scan imaging and quantitative measurement to distinguish melanoma metastasis

Jihye Baek  
Department of Electrical  
and Computer Engineering  
University of Rochester  
Rochester, NY, USA  
jbaek7@ur.rochester.edu

Shuyang S. Qin  
Department of Microbiology &  
Immunology, University of Rochester  
School of Medicine & Dentistry,  
University of Rochester, Rochester,  
NY, USA  
Shuyang\_Qin@URMC.Rochester.edu

Peter A. Prieto  
Department of Surgery, University  
of Rochester Medical Center,  
University of Rochester, Rochester,  
NY, USA  
Peter\_Prieto@URMC.Rochester.edu

Kevin J. Parker  
Department of Electrical  
and Computer Engineering  
University of Rochester  
Rochester, NY, USA  
kevin.parker@rochester.edu

**Abstract**— The H-scan analysis has been developed as a sensitive measure of ultrasound scattering types. In this study, we aim to distinguish between two different melanoma tumors: YUMM and YUMMER. To characterize the tumor tissues, H-scan was applied to the melanoma samples, resulting in estimation of several parameters. Multiparametric analysis was performed by measuring the H-scan blue fraction, attenuation coefficient, H-scan signal-to-noise ratio (SNR), and B-scan SNR. Principal component analysis was applied to the parameters, forming clusters in 2D space. These were assigned as the inputs for support vector machine (SVM) classification.

H-scan imaging was able to differentiate between YUMM and YUMMER; YUMMER showed as more blue (higher frequency) in color. The H-scan parameters of blue fraction and SNR show significant differences between the two types of melanoma. Combining the four parameters, principal components formed clusters of YUMM and YUMMER. The clusters were separated by the decision planes obtained using SVM analysis with 88.5% classification accuracy. We anticipate clinical use of H-scan parameters for melanoma diagnosis.

**Keywords**— *H-scan, Multiparametric analysis, Tissue characterization, Melanoma metastasis, Melanoma diagnosis*

## I. INTRODUCTION

Ultrasound imaging and some quantitative measurements have been developed to diagnose diseases, to differentiate between normal and abnormal tissue, and to classify disease. Specifically, shear wave speed, attenuation imaging, and quantitative ultrasound have been studied [1-8]. However, B-scan imaging is still most frequently used. Recently, the H-scan analysis has been proposed as a sensitive measure of scattering types, providing color-coded images [9]. It was found that H-scan resulted in higher accuracy than shear wave speed analysis [10]. Since the H-scan can estimate several parameters, multiparametric analysis including H-scan derived parameters has been also studied [11-13]. This multiparametric H-scan analysis is advantageous in that it utilizes frequency domain signals rather than only utilizing intensity domain analysis. Extracting more information from the frequency domain enables the detection of more sensitive changes in tissues [12]. Moreover, this multiparametric analysis based on H-scan can track disease progression by providing parameter trajectories [14].

Our goal in this study is to detect the differences within melanoma tumor microenvironments (TMEs), differentiating subtypes that are immunologically different. It is known that patients can have multiple metastases of melanoma with

different TMEs at the same time, which may result in varying responses to the same systemic treatment. Thus, non-invasive methods of classifying the melanoma TME would be helpful for treatment planning or monitoring treatment response. H-scan imaging and quantitative measurement may provide improved diagnosis to distinguish different melanoma TMEs.

We first obtained ultrasound and H-scan images and then estimated melanoma parameters based on the H-scan analysis, attenuation estimation, and B-scan intensity. Histology was performed to (1) verify the H-scan measurements and (2) show consistency between histology and H-scan. Lastly, multiparametric analysis, combining the parameters, was performed to suggest a diagnosis guideline with decision planes to separate melanoma subtypes.

## II. MATERIALS AND METHODS

### A. *In vivo animal study*

An *in vivo* study was performed in accordance with the approved guidelines of the University of Rochester's University Committee on Animal Resources. C57BL/6J mice were enrolled (Jackson Laboratory, Bar Harbor, ME, USA). One million YUMM 1.7 (Yale University Mouse Melanoma) or YUMMER 1.7 (Yale University Mouse Melanoma Exposed to Radiation) cells were implanted in the mice flanks to generate two distinct melanoma tumors. Thus, two types of melanoma were investigated in this study.

### B. *Data acquisition*

Ultrasound images were acquired using a Vevo 3100 imaging system (FUJIFILM VisualSonics, Inc., Toronto, Canada) with a 40 MHz center frequency linear transducer (MX550D). 3D volumes were obtained with a 0.05 mm step size, and then approximately 0.1 mm to 5 mm lengths were imaged. For each frame of the 3D volume data, the tumor boundary was manually contoured.

### C. *H-scan and parameter measurement*

The H-scan matched filter analysis was first applied to the signals within the region of interest (ROI) of radiofrequency (RF) data to estimate frequency components. Due to ultrasound attenuation, down-shifts in frequency were observed, enabling an estimate of the tissue's attenuation coefficient ( $\alpha$ ). Moreover, the estimated coefficient was also used to obtain attenuation-corrected RF data. The H-scan analysis was applied to the corrected RF data, resulting in the

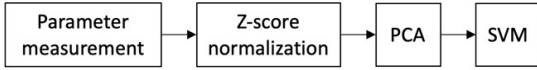


**Figure 1.** Multiparametric analysis flow chart.

fraction or percentage of higher frequency scattering encoded as blue color, which is known as percent blue (% blue):

$$\% \text{ blue} = \frac{\text{Number of blue pixels}}{\text{Total number of pixels}} \times 100. \quad (1)$$

H-scan analysis results in color levels for all pixels of input RF data. The color levels range from 1 to 256 [9]; levels 1-128 are considered red in color while levels 129-256 are considered blue in color. Thus, the number of pixels having color level between 129 and 256 is the numerator of (1). Utilizing the color levels obtained by H-scan analysis, we calculated the signal-to-noise ratio (SNR) of the color levels:

$$\text{H-scan SNR} = \mu_c / \sigma_c \quad (2)$$

where  $\mu_c$  and  $\sigma_c$  are the mean and standard deviation of the color levels, respectively. In addition to the SNR of the H-scan, we also measured the SNR of the B-scan envelope data:

$$\text{B-scan SNR} = \mu_B / \sigma_B \quad (3)$$

where  $\mu_B$  and  $\sigma_B$  are the mean and standard deviation of the envelope data, respectively. Hence, we estimated four parameters, (% blue,  $\alpha$ , H-scan SNR, and B-scan SNR). For each parameter, statistical analysis was performed.

#### D. Multiparametric analysis

H-scan and B-scan derived the four parameters, and the flow chart in **Figure 1** shows our multiparametric analysis using principal component analysis (PCA) and support vector machine (SVM) classification. The parameters have different scales, so Z-score normalization was applied to make the parameter distribution consistent with an average of 1 and a standard deviation of 0. The normalized parameters were analyzed using PCA, resulting in principal components. The first two principal components were used to show clustering results of YUMM and YUMMER data points. Lastly, with the

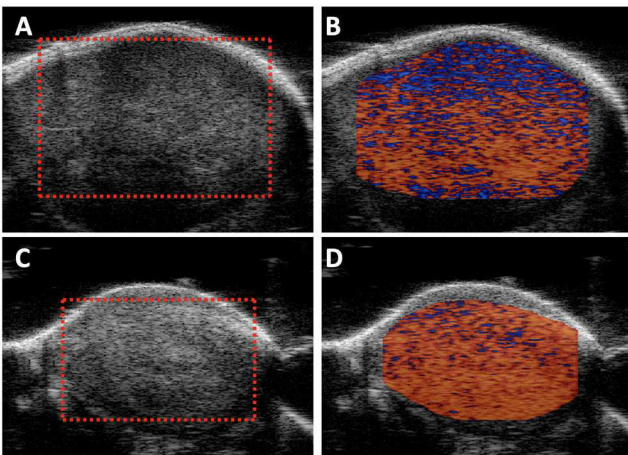


**Figure 2.** B-scan (a, c) and H-scan (b, d) imaging for YUMMER (a, b) and YUMM (c, d).

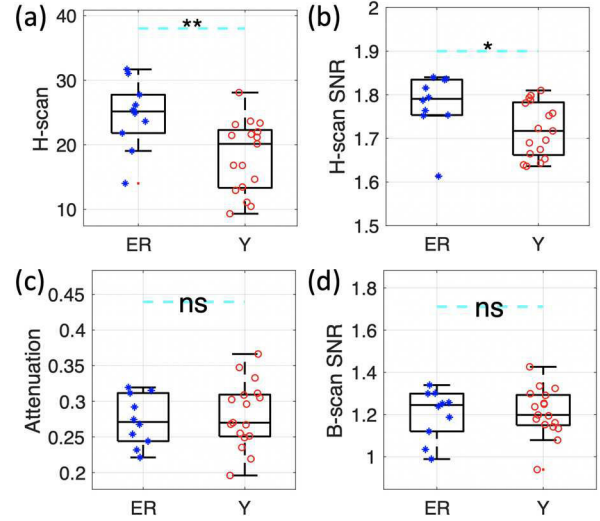


**Figure 3.** Measured features: (a) H-scan % blue, (b) H-scan SNR, (c) Attenuation coefficient [dB/MHz/cm], and (d) B-scan SNR. p-value with the following notations: \*  $p < 0.05$ , \*\*  $p < 0.01$ , \*\*\*  $p < 0.001$ , \*\*\*\*  $p < 0.0001$ , n.s. not significant

two principal components, SVM was used to construct a decision plane between the two melanoma types.

### III. RESULTS AND DISCUSSION

**Figure 2** shows B-scan and H-scan images of YUMMER and YUMM scans. The H-scan image for YUMMER displays more blue color pixels (**Figure 2 (b)**), which was quantified by the H-scan parameter, % blue. Most of the YUMM pixels in **Figure 2 (d)** show as red, whereas the YUMMER pixels show blue and red areas. Thus, the YUMM type provides more uniform color distribution compared with YUMMER, which was quantified by the SNR of the H-scan color. Including the two H-scan parameters, **Figure 3** shows the four measured parameters along with p-values. Consistent with the H-scan imaging results, YUMMER has higher % blue than YUMM, and the difference is significant. The H-scan SNR also shows significant difference between the two melanoma types. However, the attenuation coefficient and B-scan SNR show no significant difference. Therefore, the frequency-based analysis of H-scan is more sensitive in detecting the difference between melanoma subtypes compared to the intensity-based analysis of B-scan.

To unify the results of the four parameter estimation, PCA calculates the principal components as shown in **Figure 4 (a-b)**. The first principal component shows significant difference between YUMMER and YUMM. **Figure 4 (c)** shows a decision plane obtained by the SVM and clusters of YUMMER and YUMM. The clustering accuracy was assessed using SVM, resulting in a high accuracy of 88.5%, although they are both melanoma subtypes. PCA enables the visualization of all information extracted from the four parameters in 2D space, whereas the 4 parameters without applying PCA cannot be visualized in 2D or 3D space.

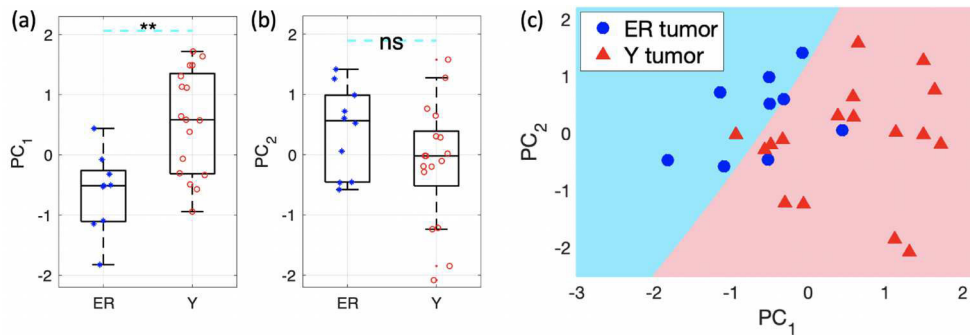


**Figure 4.** PCA and SVM results. Principal components (PC): (a) PC<sub>1</sub> and (b) PC<sub>2</sub>. (C) Clusters of YUMMER (ER) and YUMM (Y), and decision plane obtained by SVM to differentiate YUMMER and YUMM.

#### IV. CONCLUSION

The H-scan analysis is capable of distinguishing between the YUMM and YUMMER subtypes of melanoma. H-scan parameters can differentiate the subtypes with low p-value (<0.05) and high classification accuracy (88.5%), and H-scan imaging also shows a color difference between the two. This difference is not noticeable in B-scan parameters and imaging. Given that YUMMER melanoma tumors contain more immune cells within their TME than YUMM melanoma tumors, H-scan may detect the immune cell number difference [15, 16]. The potential for H-scan analysis to predict melanoma treatment response requires further investigations.

Therefore, the H-scan approach with the parameters is promising for the clinical differentiation of immunologically distinct melanoma TMEs. We anticipate clinical use of H-scan parameters for melanoma diagnosis as well as the monitoring of treatment response in heterogenous metastatic disease.

#### ACKNOWLEDGMENT

This work was supported by National Institutes of Health grant R21EB025290.

#### References

[1] K. Quiaoit, D. DiCenzo, K. Fatima *et al.*, "Quantitative ultrasound radiomics for therapy response monitoring in patients with locally advanced breast cancer: Multi-institutional study results," *Plos One*, vol. 15, no. 7, Jul 27, 2020.

[2] A. M. Pirmoazen, A. Khurana, A. El Kaffas *et al.*, "Quantitative ultrasound approaches for diagnosis and monitoring hepatic steatosis in nonalcoholic fatty liver disease," *Theranostics*, vol. 10, no. 9, pp. 4277-4289, 2020.

[3] M. L. Oelze, and J. Mamou, "Review of Quantitative Ultrasound: Envelope Statistics and Backscatter Coefficient Imaging and Contributions to Diagnostic Ultrasound," *IEEE Trans Ultrason Ferroelectr Freq Control*, vol. 63, no. 2, pp. 336-51, Feb, 2016.

[4] S. C. Lin, E. Heba, T. Wolfson *et al.*, "Noninvasive Diagnosis of Nonalcoholic Fatty Liver Disease and Quantification of Liver Fat Using a New Quantitative Ultrasound Technique," *Clinical Gastroenterology and Hepatology*, vol. 13, no. 7, pp. 1337-+, Jul, 2015.

[5] J. Mamou, and M. L. Oelze, *Quantitative ultrasound in soft tissues*, Dordrecht: Springer, 2013.

[6] R. J. Lavarello, W. R. Ridgway, S. S. Sarwate *et al.*, "Characterization of Thyroid Cancer in Mouse Models Using High-Frequency Quantitative Ultrasound Techniques," *Ultrasound in Medicine and Biology*, vol. 39, no. 12, pp. 2333-2341, Dec, 2013.

[7] M. L. Oelze, W. D. O'Brien, and J. F. Zachary, "Quantitative ultrasound assessment of breast cancer using a multiparameter approach," *2007 Ieee Ultrasonics Symposium Proceedings, Vols 1-6*, pp. 981-+, 2007.

[8] M. L. Oelze, W. D. O'Brien, Jr., J. P. Blue *et al.*, "Differentiation and characterization of rat mammary fibroadenomas and 4T1

mouse carcinomas using quantitative ultrasound imaging," *IEEE Trans Med Imaging*, vol. 23, no. 6, pp. 764-71, Jun, 2004.

[9] K. J. Parker, and J. Baek, "Fine-tuning the H-scan for discriminating changes in tissue scatterers," *Biomedical Physics & Engineering Express*, vol. 6, no. 4, Jul, 2020.

[10] J. Baek, R. Ahmed, J. Ye *et al.*, "H-Scan, Shear Wave and Bioluminescent Assessment of the Progression of Pancreatic Cancer Metastases in the Liver," *Ultrasound in Medicine and Biology*, vol. 46, no. 12, pp. 3369-3378, Dec, 2020.

[11] J. Baek, S. S. Poul, L. Basavarajappa *et al.*, "Clusters of Ultrasound Scattering Parameters for the Classification of Steatotic and Normal Livers," *Ultrasound in Medicine & Biology*, 2021.

[12] J. Baek, S. S. Poul, T. A. Swanson *et al.*, "Scattering Signatures of Normal Versus Abnormal Livers with Support Vector Machine Classification," *Ultrasound in Medicine and Biology*, vol. 46, no. 12, pp. 3379-3392, Dec, 2020.

[13] J. Baek, T. A. Swanson, T. Tuthill *et al.*, "Support vector machine (SVM) based liver classification: fibrosis, steatosis, and inflammation," *Proceedings of the 2020 Ieee International Ultrasonics Symposium (Ius)*, 2020.

[14] J. Baek, and K. J. Parker, "H-scan trajectories indicate the progression of specific diseases," *Medical Physics*, Aug 3, 2021.

[15] S. S. Qin, B. J. Han, A. Williams *et al.*, "Intertumoral Genetic Heterogeneity Generates Distinct Tumor Microenvironments in a Novel Murine Synchronous Melanoma Model," *Cancers*, vol. 13, no. 10, pp. 2293, 2021.

[16] J. Wang, C. J. Perry, K. Meeth *et al.*, "UV-induced somatic mutations elicit a functional T cell response in the YUMMER 1.7 mouse melanoma model," *Pigment cell & melanoma research*, vol. 30, no. 4, pp. 428-435, 2017.

